Experimental Verification and Simulation of Negative Index of Refraction Using Snell's Law

C. G. Parazzoli, R. B. Greegor, K. Li, B. E. C. Koltenbah, and M. Tanielian
Boeing Phantom Works, P.O. Box 3999, Seattle, Washington 98124
(Received 5 September 2002; published 11 March 2003)

We report the results of a Snell's law experiment on a negative index of refraction material in free space from 12.6 to 13.2 GHz. Numerical simulations using Maxwell's equations solvers show good agreement with the experimental results, confirming the existence of negative index of refraction materials. The index of refraction is a function of frequency. At 12.6 GHz we measure and compute the real part of the index of refraction to be -1.05. The measurements and simulations of the electromagnetic field profiles were performed at distances of 14λ and 28λ from the sample; the fields were also computed at 100λ.

DOI: 10.1103/PhysRevLett.90.107401 PACS numbers: 78.20.Ci, 41.20.Jb, 42.15.Dp, 42.25.Bs

In 1968, Veselago [1] discussed the likelihood of a negative index of refraction material (NIM). Recently, NIMs were realized by the appropriate combination of conductive and dielectric elements deposited on a substrate [2]. In the microwave regime, NIMs are fabricated from metallic wires and rings assembled in a periodic cell structure. The rings are generally referred to as split ring resonators (SRR). NIMs have the property that the effective permittivity ε_{eff} and permeability μ_{eff} are both negative. This results in an effective negative index of refraction, $n = \sqrt{\mu}\sqrt{\varepsilon}$. In a positive index of refraction material, the triplet set of vectors $\vec{E}, \vec{H}, \vec{k}$ is a right-handed set, whereas in a NIM the set is left-handed.

An experiment in a waveguide environment verifying the existence of NIMs has been reported by Shelby *et al.* [2] using Snell's law. These results were, however, criticized on theoretical grounds [3], suggesting that only the phase velocity is refracted negatively while the group velocity is refracted positively. This was rebutted [4,5] by noting, first, that Valanju *et al.* [3] considered only the electric field and neglected the Poynting vector and, second, that in an isotropic medium, two waves of different frequency and with parallel directions of propagation reveal the group velocity through an interference pattern. The normal to this interference pattern corresponds to the direction of propagation of the group velocity. However, in a dispersive medium such as NIM, waves of different frequency propagate along nonparallel directions. Under these conditions, the normal to the interference pattern no longer represents the direction of propagation of the group velocity as was erroneously assumed [3]. Our experiment and simulation fully support the results of [4,5].

In this Letter, we report that our experimental and numerical simulation results of the Snell's law confirm the presence of a negative index of refraction and are consistent with arguments made in [4,5]. The primary differences between the present work and the previous investigation [2] are (a) a free space environment is used as opposed to a waveguide measurement system, (b) data were taken at two different distances from the sample, and (c) numerical simulations showed excellent agreement with the experimental observations.

In our experiments and numerical simulations a one-dimensional (1D) NIM structure was used. A 1D structure is defined as a structure where the patterns reside on one set of parallel planes only, whereas for a 2D structure the patterns are on two sets of orthogonal parallel planes. Indeed, for the verification of NIM behavior using Snell's law, it is not necessary to use a 2D structure such as the one used previously [2]. The elementary cell structure of the 1D NIM used for our investigations was the 901 high wire density (HWD) structure shown in Fig. 1. In a 1D

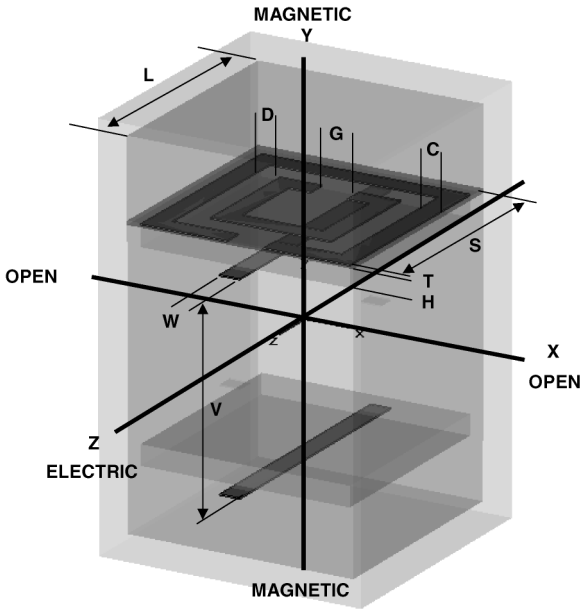

FIG. 1. Unit cell of the 901 HWD structure used in the numerical simulations. The direction of propagation of the electromagnetic field is along the x axis, the electric field is oriented along the z axis, and the magnetic field is along the y axis. $C = 0.025$ cm, $D = 0.030$ cm, $G = 0.046$ cm, $H = 0.0254$ cm, $L = 0.33$ cm, $S = 0.263$ cm, $T = 17.0 \times 10^{-4}$ cm, $W = 0.025$ cm, and $V = 0.255$ cm.

NIM, the effective permittivity and permeability tensors, in the coordinate system of Fig. 1, where x is the direction of propagation, are given, respectively, by $\overleftrightarrow{\varepsilon} = (1, 1, \varepsilon_z)$ and $\overleftrightarrow{\mu} = (1, \mu_y, 1)$. Here the SRR generates the negative permeability μ_y, and the metal strip in the z direction (the wire) generates the negative permittivity ε_z. The SRR and wire are deposited on a low loss dielectric substrate.

A typical NIM contains a large number of cells similar to the one shown in Fig. 1. The cells are stacked along the direction of propagation, x, the direction of the B field, y, and the direction of the E field, z. Direct simulation of a large number of cells is not computationally efficient. A more efficient approach, with a small penalty in accuracy, is to solve Maxwell's equations only in a single cell with appropriate boundary conditions. Once the solution of Maxwell's equations in a single cell has been found, the complex scattering parameters S_{11} (reflection) and S_{21} (transmission) in the direction of propagation are computed [6] using MICROWAVE STUDIO [7] (MWS). The types of boundary conditions available are open, electrical, magnetic, and periodic. The choice of the boundary condition mix is a function of the model geometry and will be discussed in a future publication [6].

NIMs display bianisotropy [8]. However, from our numerical simulations with 1D unit cells, we observed that this bianisotropy is weak. In view of this observation, we assume that the behavior of NIMs can be heuristically described, neglecting bianisotropy, by the effective medium theory with a permittivity tensor $\overleftrightarrow{\varepsilon} = (1, 1, \varepsilon_z)$ and permeability $\overleftrightarrow{\mu} = (1, \mu_y, 1)$. These parameters are obtained from the computed or measured scattering parameters [6] using

$$S_{11} = \frac{(-1 + e^{2idk_0n})(-1 + Z^2)}{-(-1 + Z)^2 + e^{2idk_0n}(1 + Z)^2}$$

$$\text{and} \quad S_{21} = \frac{4e^{idk_0n}Z}{-(-1 + Z)^2 + e^{2idk_0n}(1 + Z)^2},$$

where k_0 is the free space wave-vector modulus, $n = \sqrt{\mu}\sqrt{\varepsilon}$ is the index of refraction, $Z = \sqrt{\mu}/\sqrt{\varepsilon}$ is the impedance, and d is the sample thickness.

As shown in Fig. 2, for the Snell's law experiment, the detector of the electric field is placed at 33 and 66 cm from the entrance face of the NIM wedge. The radiation from a rectangular waveguide feeds a conical horn. A lens is located at the exit of the horn. The lens illuminates the NIM sample (wedge) with either a focused or collimated beam. The operational frequency range of the apparatus is between 8.0 and 20 GHz. For the execution of the Snell's law experiment a NIM wedge sample was located in the focal region. The orientation of the wedge was such that the incident radiation was deflected in the x-y plane. The detector was moved on a circular arc centered on the backside of the wedge.

The electromagnetic beam illuminates the wedge through a rectangular aperture (not shown in Fig. 2) of 12.7 cm. The wedge angle is 32.19°. The unit cell dimension of the NIM in the direction of propagation is 0.33 cm. The short side of the wedge contains five cells; the long side contains 32 cells. The average thickness of the wedge in the direction of propagation x is 6.10 cm. In addition to the 1D NIM wedge, an identical wedge made of Teflon was also built for calibration purposes.

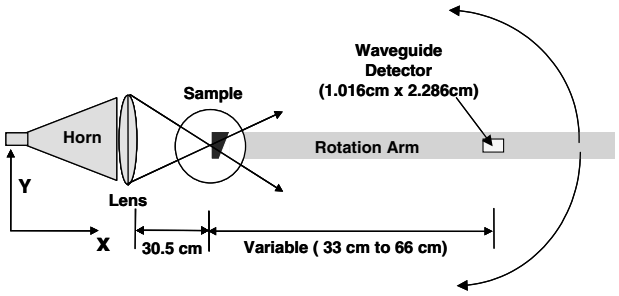

FIG. 2. Schematic of the setup used in the Snell's law experiment showing the conical horn, lens, sample, and waveguide detector. The measurements were made in the focused and collimated mode at 33 and 66 cm away from the sample.

The simulation of the fields in the proximity of the NIM wedge was performed using the effective medium theory and the "*ab initio*" solvers of Maxwell's equations, MWS and MAFIA [6,7]. The effective permittivity and permeability tensors were obtained, as described above, from the MWS computed scattering parameters of the 901 HWD structure. The far field was obtained using the Helmholtz-Kirchhoff theorem [6].

A bulk material, 1D structure was simulated in MAFIA using the MWS derived effective permittivity and permeability. The effective permittivity and permeability tensors, at 12.6 GHz, were $\overleftrightarrow{\varepsilon} = (1, 1, -1.8922 - 0.0001i)$ and $\overleftrightarrow{\mu} = (1, -0.5775 - 0.0045i, 1)$. A Lorentz [9] dispersion model was used to represent each component of the permittivity and permeability tensors as a function of the frequency f. The illuminating electromagnetic pulse polarized in the x direction was nearly monochromatic with bandwidth $\Delta f/f = 10^{-6}$.

The results of the numerical simulations are shown in Fig. 3. The pulse travels from left to right, in the positive x direction. The contour plots of the E_z component of the electric field are shown both for the Teflon (reference) and the NIM wedges. The wave fronts emerging from the wedge are clearly deflected in opposite directions for the two materials. Observe that in our simulations a nearly monochromatic source was used; therefore, the normal to the interference patterns correctly represent the direction of the group velocity [4]. We explored numerically the effect of increasing the material losses. The losses were increased up to 2 orders of magnitude over the experimentally observed values. The computed refracted angle was nearly unchanged by the losses.

In Fig. 4(a) we show the contour plots of the x component of the Poynting vector, $P_x(x, y = 0, z = 0, t)$, in the x-t plane for the Teflon case. The slope of the fringes is the phase velocity, $dx/dt = 2\pi f/nk_0 = c/n$. As expected,

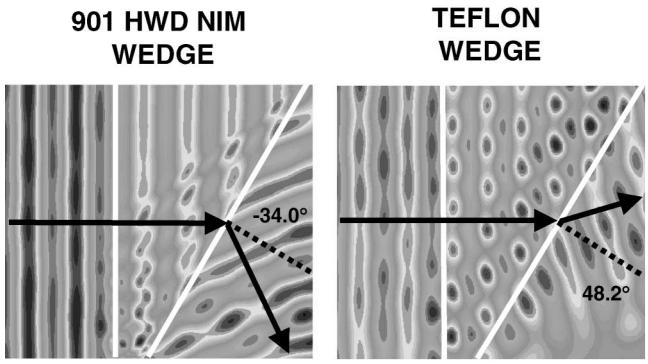

FIG. 3. Contour plots, in the $z = 0$ plane (medium plane of the experiment), of the E_z component of the electric field as computed by MAFIA at 12.6 GHz. The radiation propagates from left to right. The wedge angle is 32.19°. Left: NIM wedge $n = \{-1.0454 - 0.0041\}$ $(i, \varepsilon = \{1, 1, -1.8922 - 0.0001i\}, \quad \mu = \{1, -0.5775 - 0.0045i, 1\})$. Right: Teflon wedge $n = 1.4$.

the phase velocity decreases in the Teflon wedge. Similar results are presented in Fig. 4(b) for the NIM wedge. Observe that the phase velocity reverses its sign in the NIM wedge, but the Poynting vector is always directed in the positive x direction as expected.

In Fig. 5 we present the measured normalized amplitude, $E_z(r, f)$, of the z component of the electric field as a function of the detector angle r and frequency f. The refraction angle r is measured from the normal of the wedge exit face and is positive in the counterclockwise direction. The refraction angle $r_{\max}$ is defined as $[\partial E_z(r, f)/\partial r]_{r=r_{\max}} = 0$. In Fig. 5 the response of the Teflon and NIM 901 HWD wedges are shown. As expected, the Teflon refraction angle $r_{\max} > 0$ is constant. On the contrary, $r_{\max} < 0$ for the NIM wedge and is strongly dependent on the frequency. These results have been duplicated [10] at another lab utilizing our NIM sample, but with a different experimental setup having a sample to detector distance of ~450 cm.

We performed a quantitative comparison between the measured and computed $E_z(r, f = 12.6\ \text{GHz})$ angular profiles at a single frequency for two detector locations,

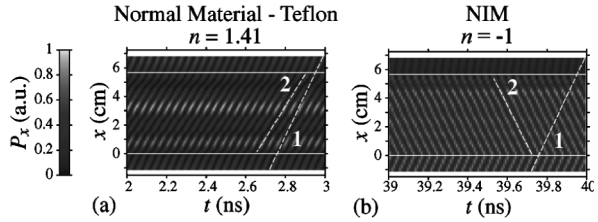

FIG. 4. Plots P_x $(x, y = 0, z = 0, t)$ showing contours of constant phase velocity simulations for (a) the Teflon wedge and (b) the NIM wedge. The solid horizontal lines denote the edges of the wedge, and the dashed lines highlight the fringe slopes that represent the phase velocities: (1) corresponds to c, the phase velocity in vacuum; (2) corresponds to c/n, the phase velocity in the respective materials.

33 and 66 cm away from the sample. The experimental results for the two locations are shown in Fig. 6(a). We obtained the computed values of the angular profiles by applying the Helmholtz-Kirchhoff propagator to the MAFIA computed fields at the exit face of the wedge. The comparison of the simulations to the experimental data at 33 cm is shown in Fig. 6(b). The agreement between the computed and measured data is quite good. The refraction angle $r_{\max}$ for Teflon is correctly computed and measured at 48.21°, as expected from Snell's law for a 32.19° wedge with $n = 1.4$. Similarly, the computed and measured refraction angle for the NIM wedge at 12.6 GHz ($n = -1.0454$) is also in good agreement. The angular profiles of the Teflon and NIM wedges are similar at two distances from the detector. This indicates that the radiation field exiting the NIM wedge propagates in the same manner as the one from the Teflon wedge, the only difference being the negative angle of refraction. In Fig. 6(b) the computed angular profile of $E_z(r, f = 12.6\ \text{GHz})$ at 238.1 cm (100 wavelengths) is also given. We observe that the broadening of the angular profile for the NIM wedge due to dispersion effects is negligible and the observed behavior of the NIM wedge cannot be explained by dispersion effects alone as previously suggested [3], but can be explained only by the presence of a negative index of refraction. The broadening is given by

$$\Delta r = \frac{\sin(i)}{\sqrt{1 - n_0^2 \sin^2(i)}} \left(\frac{dn}{df}\right)_{f=f_0} f_0 \left(\frac{\Delta f}{f_0}\right),$$

where $i = 32.19°$ is the wedge angle; $n_0 = -1.0454$ is the NIM index of refraction at $f_0 = 12.6$ GHz; $(dn/df)_{f=f_0} \approx 1.0\ \text{GHz}^{-1}$ is the slope of the NIM sample

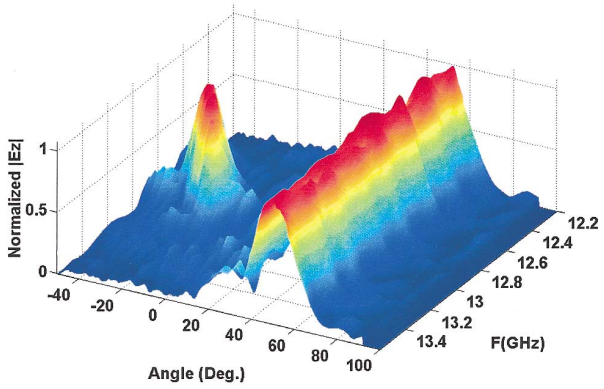

FIG. 5 (color). Surface plot of measured normalized peak amplitude of electric field component $E_z(r, f)$ for the Teflon and 901 HWD NIM wedge. Note that the electric field refracted by the Teflon wedge peaks at a positive refractive angle of 48.2° (corresponding to an index of refraction of 1.4) and is independent of frequency. The electric field refracted by the NIM wedge, however, peaks at negative angles that are a function of the frequency. The two peaks are not normalized by the same factor. The non-normalized value of the peak electric field of the NIM sample is about 20% of the Teflon peak.

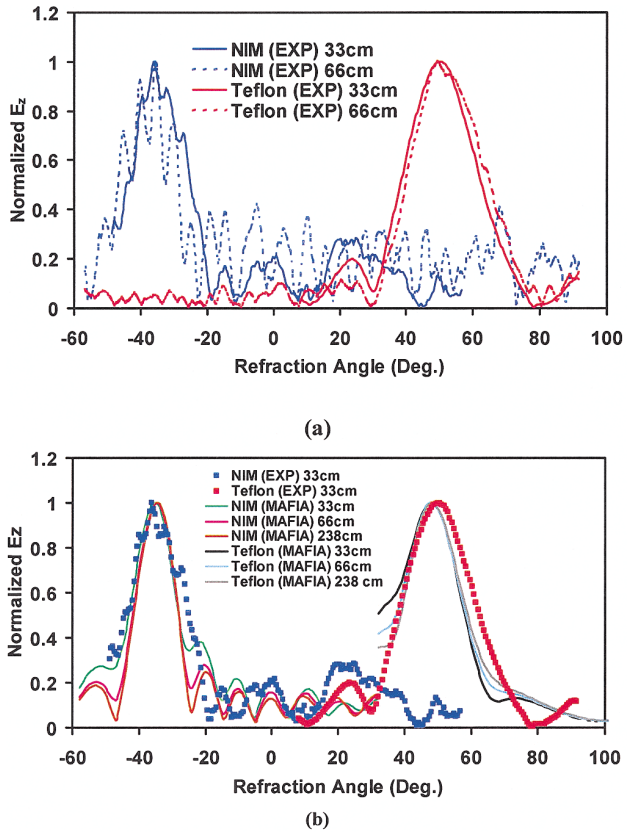

FIG. 6 (color). (a) Measured angular profile of the normalized electric field amplitude $E_z(r)$, at a constant frequency $f = 12.6$ GHz for detector distances of 33 and 66 cm from the Teflon and 901 HWD NIM wedges. (b) Measured 33 cm data compared to simulated results at 33, 66, and 238 cm (100λ) from the Teflon and 901 HWD NIM wedges.

dispersion curve (Fig. 7); and $(\Delta f/f_0) = 10^{-6}$ is the bandwidth of the illuminating fields. With the above values, we find the broadening, $\Delta r \approx 5 \times 10^{-4}{}^\circ \ll 1^\circ$, to be negligible.

Finally, we evaluated the index of refraction dispersion relation $n_{\mathrm{Th}}^{\mathrm{NIM}}(f)$ for the NIM wedge, from the MWS computed values of the scattering parameters. The values of $n_{\mathrm{Th}}^{\mathrm{NIM}}$ obtained were compared with the values $n_{\mathrm{Ex}}^{\mathrm{NIM}}$ derived from Snell's law using the experimentally observed position of the refraction angle $r_{\max}$. Specifically, we used the relation $n_{\mathrm{Ex}}^{\mathrm{NIM}} = \sin(r_{\max})/\sin(i)$. The results are shown in Fig. 7. The agreement over the 12.2 to 13.6 GHz frequency range is within experimental error.

In summary, we report the results of a Snell's law experiment on a NIM wedge. Measurements and simulations were performed at two different distances from the sample. The results support the observations reported by Shelby *et al.* for measurements done in a waveguide

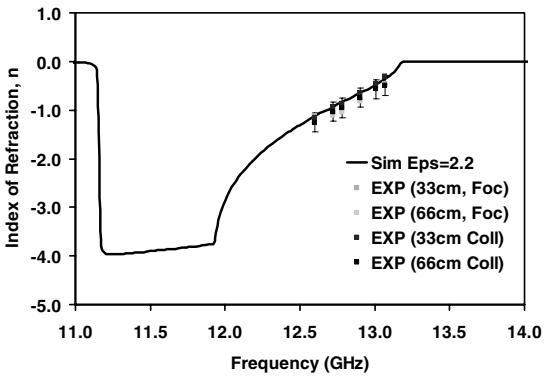

FIG. 7. Experimental and computed dispersion relation of the index of refraction for the 901 HWD structure with substrate $\varepsilon = 2.2$. The experimental data were taken in both the focused and collimated beam setup at 33 and 66 cm from the wedge.

environment using a somewhat different sample. The data clearly confirm the existence of a negative index of refraction for a specific frequency window and thus the existence of NIMs.

This work was supported by DARPA Contract No. MDA972-01-2-0016. We extend our thanks to V. Starkovich, S. Mclean, J. Nielsen, and A. Vetter from Boeing, S. Schultz and D. Smith from the University of California–San Diego, C. Soukoulis and P. Markos from Iowa State University, and R. Schuhmann and T. Weiland from Technical University of Darmstadt for useful discussions, suggestions, and help with various aspects of this work.

[1] V. G. Veselago, Sov. Phys. Usp. **10**, 509 (1968).
[2] R. A. Shelby, D. R. Smith, and S. Schultz, Science **292**, 77 (2001).
[3] P. M. Valanju, R. M. Walser, and A. P. Valanju, Phys. Rev. Lett. **88**, 187401 (2002).
[4] J. B. Pendry and D. R. Smith, Appl. Phys. Lett. (to be published).
[5] J. Pacheco, T. M. Grzegorczyk, B. I. Wu, Y. Zhang, and J. A. Kong, Phys. Rev. Lett. **89**, 257401 (2002).
[6] C. G. Parazzoli, R. B. Greegor, B. E. C. Koltenbah, and M. Tanielian (to be published).
[7] T. Weiland, R. Schuhmann, R. B. Greegor, C. G. Parazzoli, A. M. Vetter, D. R. Smith, D. C. Vier, and S. Schultz, J. Appl. Phys. **90**, 5419 (2001).
[8] R. Marques, F. Medina, and R. Rafii-El-Idrissi, Phys. Rev. B **65**, 144440 (2002).
[9] A. Taflove and S. C. Hagness, *Computational Electrodynamics* (Artech House, Boston, 2000), 2nd ed.
[10] T. Schaefer, Mayo Clinic (private communication).